Internal Power Flow Control For Modular Multilevel Converter During Submodule Failure

Hashfi, Tuanku Badzlin; Vahedi, Hani; Palensky, Peter; Lekić, Aleksandra

DOI
10.1109/PowerTech59965.2025.11180269

Publication date
2025

Document Version
Final published version

Published in
2025 IEEE Kiel PowerTech, PowerTech 2025

Internal Power Flow Control For Modular Multilevel Converter During Submodule Failure

Tuanku Badzlin Hashfi, Hani Vahedi, Peter Palensky, Aleksandra Lekić
Electrical Sustainable Energy
Delft University of Technology
Delft, Netherlands
Corresponding author: t.b.hashfi@tudelft.nl

2025 IEEE Kiel PowerTech | 979-8-3315-4397-6/25/$31.00 ©2025 IEEE | DOI: 10.1109/PowerTech59965.2025.11180269

***Abstract*—The modular multilevel converter (MMC) uses many power electronic components in the high voltage direct current (HVDC) application. One of the major concerns in half-bridge MMC is the fault in the converter submodules. It raises the question of whether the reliability and high-quality performance of the MMC can be increased significantly as the active device controls the power flow between the AC- and DC-sides. During the SM fault within the MMC leg, the unbalance is introduced inside the MMC converter. The unbalanced voltage within the leg of the MMC will continuously introduce an AC-current component on the DC-side of the converter. Thus, the hybrid proportional-internal (PI) control and proportional-resonant control (PR) is introduced in controlling the power flow within the internal MMC to eliminate the AC-current component and ensure pure DC-current in the internal MMC. This study investigates the internal power flow control of a three-phase rectifier MMC with symmetric and asymmetric SM fault conditions. Compared with conventional control methods, the proposed control can tolerate SM faults and eliminate the AC-current component within the converter, increasing the converter's performance. Simulation results are included and discussed to verify the proposed control.**

***Index Terms*—Modular multilevel converter (MMC), submodule fault-tolerant control, leg-arm balancing control.**

I. Introduction

Modular multilevel converters (MMCs) have been selected as a highly interesting topology for high-voltage direct current (HVDC) applications because of their various advantages, such as modularity scheme, easy-to-balance voltage capacitor, and scalability to various voltage levels. The modularity scheme in the MMC provides less production cost and easier maintenance [1]. However, the reliability and robustness of control strategies remain quite challenging, as this topology has been widely used for HVDC networks.

To raise voltage levels in high-voltage applications like HVDC networks, MMCs need many submodules (SMs). As a result, some issues known as device or internal defects may arise inside an SM. Several redundancy SM strategies have been proposed in [2]–[5]. According to [6], all these tactics have been categorized into four (four) strategies: basic redundancy, additional redundancy SM, optimized additional redundancy SM and redundancy based on spare SM.

This work has received funding from the European Union's MSCA Doctoral Network Inter-oPEn under grant agreement No. 101119349. Views and opinions expressed are however those of the author(s) only and do not necessarily reflect those of the European Union or REA. Neither the European Union nor the REA can be held responsible for them.

SM fault tolerance has often been achieved with phase-shifted pulse width modulation (PS-PWM) [5]–[7]. Each SM has its carrier wave in this technique, which is phase-shifted from the other SM carriers. However, this modulation method has lower line-to-line output voltage spectra [8]. The nearest level modulation (NLM) technique was employed in the papers [3] and [9] to regulate the converter, causing a high fluctuation in the voltage capacitors. Using a zero-sequence offset voltage, the authors demonstrated fault tolerance by altering the reference signals. In [10], [11] proposed an attractive method by modifying phase disposition PWM (PDPWM) with an adaptive carrier. However, the proposed method was performed on a single-phase converter; thus, this approach misses out on the analysis of three-phase converters. Furthermore, the other main issue in implementing these redundancy strategies to tolerate SM faults is how the control reacts to the unbalanced voltage in the MMC legs. The energy / voltage imbalance affects the quality output of the converter.

Some control structures have been conducted to ensure the stability of the MMC during unbalanced power and / or energy in the legs [12]–[14] due to the unbalanced distributed source in each SM. However, only a few studies have investigated the effect of fault-tolerant operation and minimized the effect. Therefore, this paper focuses on the internal power flow control strategy to reduce the AC-current component of the internal MMC caused by SM faults. The hybrid proportional-integral (PI) and proportional-resonant (PR) controller is used to stabilize the power-sharing among the SM and eliminate the AC-current component during the unbalanced internal voltage SM caused by SM fault. This paper achieves internal power flow control during the SM fault in the three-phase MMC system using the adaptive-carrier PDPWM (AC-PDPWM) proposed in [10], and extended to cover the three-phase operation.

The content of this paper is organized as follows: Section II presents the mathematical model of the MMC. Then, section III presents the SM fault tolerance strategy and the leg power flow control strategies to minimize the effect of the unbalanced voltage. Section IV discusses the simulation results. Finally, Section V concludes the study.

II. Mathematical Model of MMC

The main feature of MMC is the number of cascaded/modularity connections of SMs. As seen in Figure 1, a half-bridge SM consists of two switches and a capacitor. The converter is composed of N SMs per arm, and each leg has two arms: the upper and lower arms. The two possible values of the SM voltage are V_c (the voltage in the SM capacitor) and 0 V, which are determined by the two states of each SM (that is, "ON" or inserted and "OFF" or bypassed). The bypass switch is then frequently used to bypass the SM if it is permanently unhealthy. Inductors are positioned in the center of each converter arm to act as internal filters and to balance out the voltage imbalance caused by the series of SMs' upper and lower voltage accumulation.

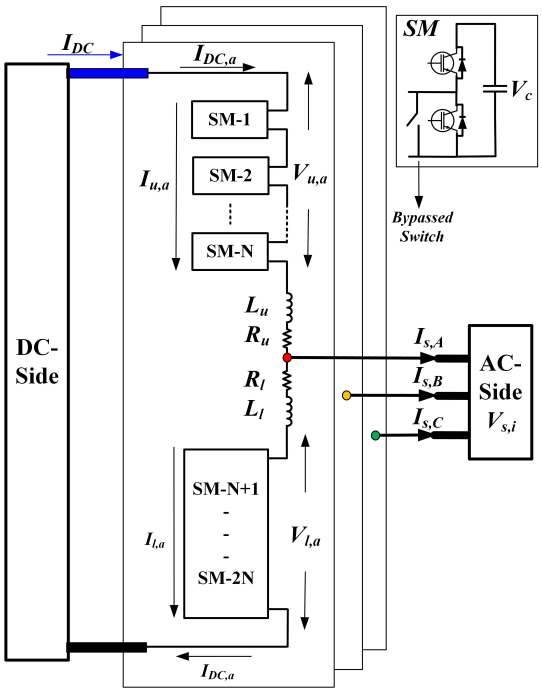

Fig. 1: Schematic of the MMC topology.

Theoretically, the output voltage is controlled by the upper (V_u) and lower voltage (V_l) sources which are sinusoidal voltages with a magnitude of up to half of the DC link voltage. Thus, according to Kirchhoff's voltage law, the AC converter voltage (V_s) can be defined as:

$$V_{s,i} = \frac{1}{2}[V_{l,i} + L_l \frac{dI_{l,i}}{dt} + I_{l,i}R_l] - \frac{1}{2}[V_{u,i} + L_u \frac{dI_{u,i}}{dt} + I_{u,i}R_u] \quad (1)$$

where $i \in \{a, b, c\}$. Again, according to Kirchhoff's current law (KCL), the AC converter current (I_s) ideally can be expressed as:

$$I_{s,i} = I_{u,i} - I_{l,i}. \quad (2)$$

Practically, the parasitic upper resistor (R_u) and lower resistor (R_l), and upper inductor (L_u) and lower inductor (L_l) are identical for all arms and legs. Since they are identical to each other, so $R_u = R_l = R$ and $L_u = L_l = L$. Thus, the AC converter voltage $V_{s,i}$ can be expressed as (3) by substituting (2) in (1):

$$V_{s,i} = (V_{l,i} - V_{u,i}) - \frac{L}{2}\frac{dI_{s,i}}{dt} - \frac{R}{2}I_{s,i}. \quad (3)$$

Regulating the SM voltages at each arm of the MMC is necessary to balance the upper voltage source and lower voltage source arms to attain converter stability. Based on KVL, the DC-side loop can be expressed as follows:

$$V_{DC} = [V_{l,i} + L_l \frac{dI_{l,i}}{dt} + I_{l,i}R_l] + [V_{u,i} + L_u \frac{dI_{u,i}}{dt} + I_{u,i}R_u] \quad (4)$$

Based on KCL, the DC-current ($I_{DC,i}$) at each leg ideally can be expressed as follows:

$$I_{DC,i} = \frac{I_{u,i} + I_{l,i}}{2}. \quad (5)$$

Substituting (5) into (4) yields:

$$V_{DC} = (V_{l,i} + V_{u,i}) + 2L\frac{dI_{DC,i}}{dt} + 2RI_{DC,i}. \quad (6)$$

Based on the equation (6), the circulating voltage can be expressed as:

$$V_{circ,i} = 2L\frac{dI_{DC,i}}{dt} + 2RI_{DC,i}. \quad (7)$$

In steady state conditions, as indicated by equation (7), the circulating voltage $V_{circ,i}$ is approximately zero. So, each phase or leg of the MMC expresses a purely DC behavior during steady-state conditions.

III. Principle Operation and Control Structure

By adding and subtracting equation (1) and equation (4), the voltage of the upper and lower arm can be formalized as:

$$V_{u,i} = \frac{V_{DC}}{2} - V_{s,i} - V_{circ,i}, \quad (8a)$$

$$V_{l,i} = \frac{V_{DC}}{2} + V_{s,i} - V_{circ,i}. \quad (8b)$$

where the AC converter voltage, $V_{s,i}$, is the voltage required to regulate the AC output current, $I_{s,i}$, and the circulating voltage, $V_{circ,i}$, is used to regulate the circulating current, $I_{circ,i}$. Then, the reference signals of the upper arm ($V_{u,i}$) and the lower arm ($V_{l,i}$) have a phase shift of $180°$ according to the expressions of (8a and 8b). In the PWM technique, the reference signals are compared with the specified carriers, which are the specific pulses sent to the SMs. This work used the AC-PDPWM [10] that can perform fault-tolerant capability to correct the carrier structure during the SM fault. The extended implementation of this method is applied in the three-phase system in this work.

Three scenarios of failure can be evaluated, which are asymmetrical failure (AF), phase symmetrical failure (PSF), and converter symmetrical failure (CSF) [6]. This work evaluates the AF and PSF and the effect of the internal power flow within the phases and arms. This paper is not focused on detecting and locating the fault. A brief explanation of the flow detecting the faulty SM can be sensed by the sensor at each SM. Then,

the fault signal will be sent to the controller and the faulty SM will be deactivated. Thus, the control only works for healthy SM. A new number of SMs is generated, and the behavior of the pulse distribution changes.

A. The Aggregate and differential upper and lower arm power control

Based on equation (2) and (5), the upper current and the lower current can be expressed:

$$I_{u,l,i} = I_{DC,pure,i} + I_{\Delta,i} + \frac{I_{s,i}}{2}, \tag{9a}$$

$$I_{u,l,i} = I_{DC,pure,i} + I_{\Delta,i} - \frac{I_{s,i}}{2}. \tag{9b}$$

In the practical case, the DC-current ($I_{DC,i}$) that flows in each leg consists of a pure DC-current ($I_{DC,pure,i}$) and an AC-current component ($I_{\Delta,i}$). The pure DC-current facilitates power transfer between the phase legs and the DC link. The AC-current component is key in transferring power to the upper and lower arms. However, the AC-current component can be included to yield additional circumstances, such as an even harmonic frequency component due to the ripple of the capacitor voltage and a fundamental frequency component due to unbalanced arm energies [14]. In a normal steady state, the AC-current components must be close to zero ($I_{\Delta,i} = 0$) to produce continuous enhanced conversion efficiency.

During SM failure, the internal power flow problem introduces more challenges to the control structure. To identify the problem, the information that the extracted energy of each SM depends on the SM voltage level is used. However, the total energy at each of the three converter legs must be equal to enable the injection of balanced currents into the grid and maintain the stability energy/voltage SM even though they are not balanced. Then, the differential energy between the upper and lower arms must be zero [14]. This can be analyzed from the equations (10a) and (10b).

$$\begin{aligned}\int P_{u,i}(t)dt = W_{u,i} &= \frac{1}{2}C_{eqv}\sum_{n=1}^{N-N_f} V_{c,u,n,i}^2 \\ &\approx \frac{C_{eqv}}{2(N-N_f)}(\sum V_{c,u,n,i})^2,\end{aligned} \tag{10a}$$

$$\begin{aligned}\int P_{l,i}(t)dt = W_{l,i} &= \frac{1}{2}C_{eqv}\sum_{n=1}^{N-N_f} V_{c,l,n,i}^2 \\ &\approx \frac{C_{eqv}}{2(N-N_f)}(\sum V_{c,l,n,i})^2.\end{aligned} \tag{10b}$$

Equations (10a) and (10b) represent the relationship of power and the amount of energy stored in each arm. N_f represents the faulty SM. The faulty SM will change the equivalent capacitance (C_{eqv}). Thus, it changes the amount of energy stored in each arm. To achieve complete control of power flow within an MMC, it is essential to enable independent power transfer between each phase's upper and lower arms. This is achieved using the fundamental frequency difference current, which governs the power exchange between the phase arms. For three-phase systems, minimizing circulating currents is crucial to maximize conversion efficiency. Thus, the fundamental frequency difference current allows independent inter-arm power transfer without affecting the grid current or introducing fundamental frequency components into the DC-side.

When SM fails, the MMC leg current becomes non-zero, and a certain amount of power is transferred through the converter legs and arms. This can be seen in the upper and lower arm powers. The average absorbed power of the upper and lower SM capacitors can be calculated by multiplying the voltages of the upper and lower phase arm ($V_{u,l,i}$) and the current ($I_{u,l,i}$). The following expressions are stated:

$$\begin{aligned}P_{u,l,i} = \frac{1}{2}\left[V_{DC}I_{DC,pure,i}\right] &\mp V_{s,i}I_{DC} \\ &+\frac{V_{DC}I_{DC,pure,i}}{4} - \frac{V_{s,i}I_{s,i}}{2},\end{aligned} \tag{11}$$

In steady state, the absorbed power consists of pure DC power and pure sinusoid AC power. The summation (Σ) and subtraction (Δ) of the integration upper power $P_{u,i}$ and lower power $P_{l,i}$ can be stated as:

$$\int P_i^{\Sigma} = W_i^{\Sigma} = W_{0,i}^{\Sigma} - \frac{V_{s,i}I_{s,i}}{4\omega_1}sin(2\omega_1 t - \theta), \tag{12a}$$

$$\begin{aligned}\int P_i^{\Delta} = W_i^{\Delta} = W_{0,i}^{\Delta} &- \frac{V_{DC}I_{s,i}}{4\omega_1}sin(\omega_1 t - \theta) \\ &- \frac{2V_{s,i}I_{DC}}{2\omega_1}sin(\omega_1 t),\end{aligned} \tag{12b}$$

where the integration constant $W_{0,i}^{\Sigma} = \frac{CV_{DC}}{N}$ and $W_{0,i}^{\Delta} = 0$ are the mean values. Equations 12a and 12b are noted because the aggregate energy ripple is twice the fundamental frequency, while the differential energy ripple is of the fundamental frequency.

Equations (12a) and (12b) can be simplified according to Equations (10a) and (10b) where the energy is proportional to capacitance and voltage. The expression is shown as follows:

$$V_c^{\Sigma} \approx 2V_{DC} - \frac{NV_{s,i}I_{s,i}}{CV_{DC}4\omega_1}sin(2\omega_1 t - \theta), \tag{13a}$$

$$\begin{aligned}V_c^{\Delta} \approx \frac{N}{CV_{DC}}[&\frac{V_{DC}I_{s,i}}{2\omega 1}sin(\omega_1 t - \theta) \\ &- \frac{2V_{s,i}I_{DC}}{\omega_1}sin(\omega_1 t)],\end{aligned} \tag{13b}$$

where, $V_c^{\Sigma} = V_{c,u,i} + V_{c,l,i}$ and $V_c^{\Delta} = V_{c,u,i} - V_{c,l,i}$. Regarding equations (13a) and (13b), if the faulty SM is bypassed, the equivalent capacitance in the specific arm can be changed and create an imbalance in the energy between the upper and lower arm. Thus, any oscillation in the SM capacitor voltages due to the imbalanced SM produces an AC frequency component on the DC-side.

B. The control structure

In an MMC, undesirable harmonic difference currents are suppressed and AC-currents components are minimized to optimize conversion efficiency. Proportional-resonant (PR) controllers are used to control harmonics, which can result from

steady-state fundamental difference currents that are absent from standard MMCs [15]. By regulating both amplitude and phase, these controllers, which are renowned for their capacity to manage both positive and negative sequence currents, effectively control harmonic components. The DC-current is then controlled by the proportional-integral (PI) controller to allocate power to each leg phase. To maintain uneven SM voltages and ensure MMC power balance, the control feedback is exclusively dependent on the total SM capacitor voltages of the arms.

As seen in Figures 2 and 3, respectively, the MMC control structure is made up of circulating current controllers and grid current controllers. The circulating current controllers work in the $\alpha\beta 0$ frame, whereas the grid controllers control active and reactive power in the $dq0$ frame. Specialized modules for managing DC, fundamental components (ω_1), second harmonic ($2\omega_1$), and third harmonic current ($3\omega_1$) are included with each axis controller. Fundamental and third-harmonic currents caused by the fundamental AC-current component are removed to increase converter efficiency, while second-harmonic currents are suppressed to reduce SM voltage ripple.

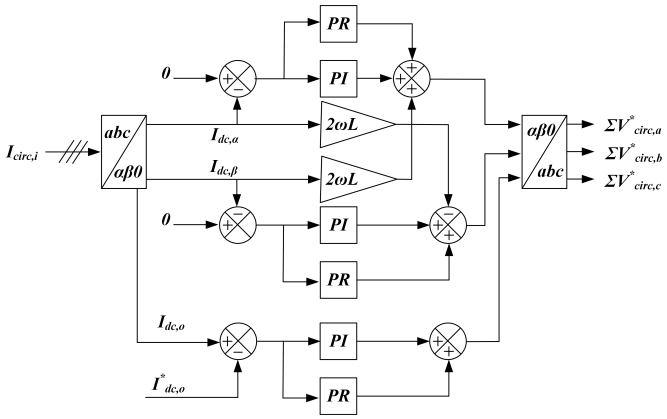

Fig. 2: Circulating suppressing current control.

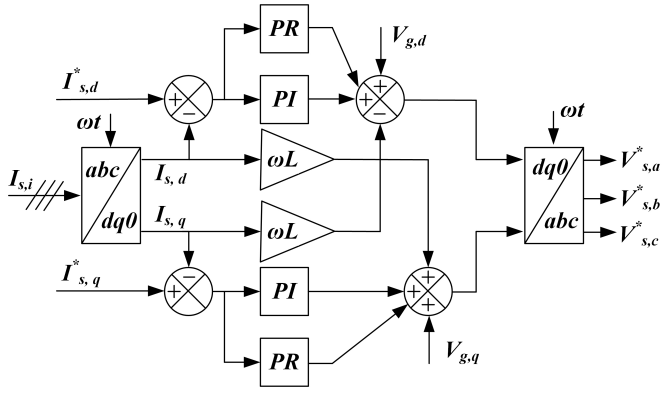

Fig. 3: Double synchronous reference frame output current controller.

The DC power and differential power of each phase are achieved through separate reference generation systems. Figure 4 illustrates how these systems use feedback based on the total voltages of the SM capacitors of the phase arms to generate references for fundamental frequency and differential currents. To maintain power balance and maximize system performance, the fundamental frequency difference current references minimize the AC-current component while guaranteeing voltage balance between the upper and lower arms.

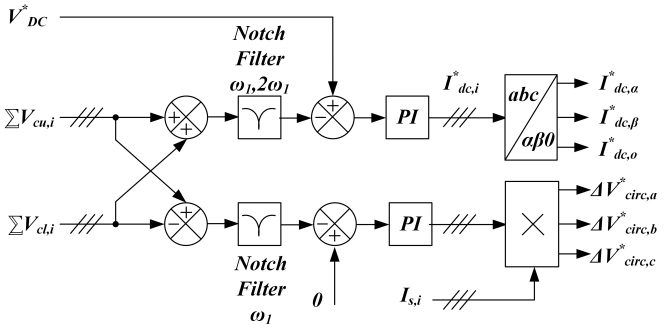

Fig. 4: Aggregate and differential leg voltage balancing control.

The sum of the aggregate and differential leg voltage balancing control will perform the circulating voltage that is used to control the AC-current component in the internal MMC as stated in equation (14). Finally, the voltage of the upper and lower arms can be controlled as stated in equation (**??**).

$$V_{circ,i} = \Sigma V_{circ,i} + \Delta V_{circ,i}. \tag{14}$$

IV. Simulation Verification

To confirm the performance of the MMC topology with the asymmetrical fault (AF) scenarios of the proposed and conventional control scheme and the phase symmetrical fault (PSF) scenarios, a three-phase MMC model is set up in MATLAB / Simulink. The converter makes use of the resistive DC load. Table I presents the simulation parameters.

TABLE I: The Parameters of Three Phase MMC under Simulation Study.

Parameter	Value	Parameter	Value
Power Rating	3.6 kW	Grid Voltage (L-N)	275 V
Grid Inductance	2.5 mH	Grid Frequency	50 Hz
DC-link Voltage	600 V	Arm Inductance	5 mH
SM Capacitance	1 mF	Number of SM per arm	4
Resistive DC Load	100 Ω	Switching Frequency	2.5 kHz

The proposed control structure is tested to verify its effectiveness by comparing it with the conventional method. This topic presents comparative investigations between the suggested internal power flow control strategy and the conventional control strategy. The results of the conventional method are shown in Figures 5 - 7. Between 0.5 and 1.5 seconds in the leg of phase-A, the SM failures occur. At 0.5 seconds, the converter first encounters an AF in SM-1 in the upper arm. Accordingly, as seen in Figure 5(a), the converter lowers the voltage at phase-A by one level, from 9-level to 8-level.

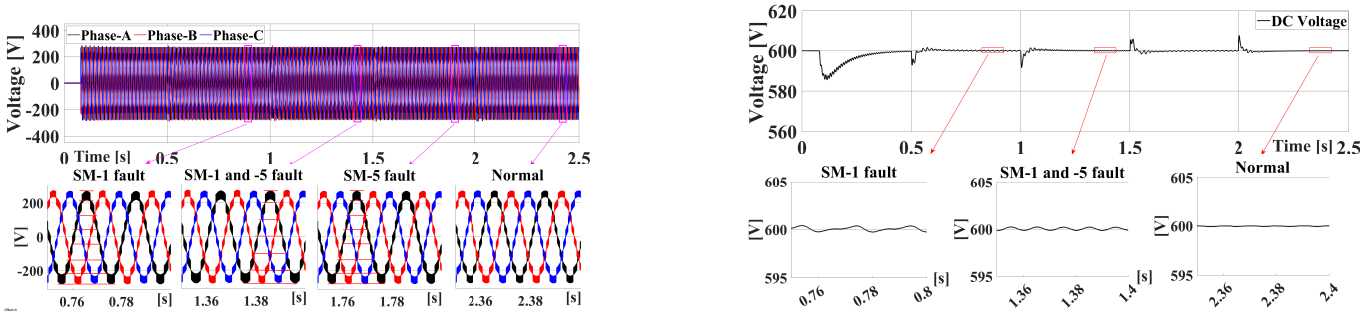

(a) (b)

Fig. 5: (a) The three-phase AC converter voltages and (b) the DC voltage using conventional method.

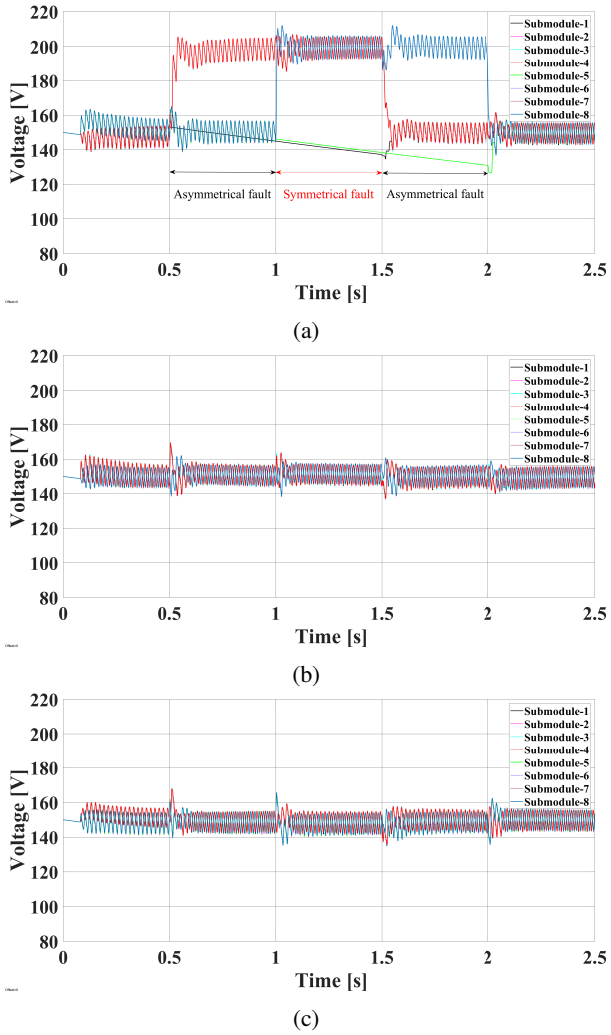

(a) (b) (c)

Fig. 6: SM capacitor voltages at (a) first leg, (b) second leg, and (c) third leg using conventional method.

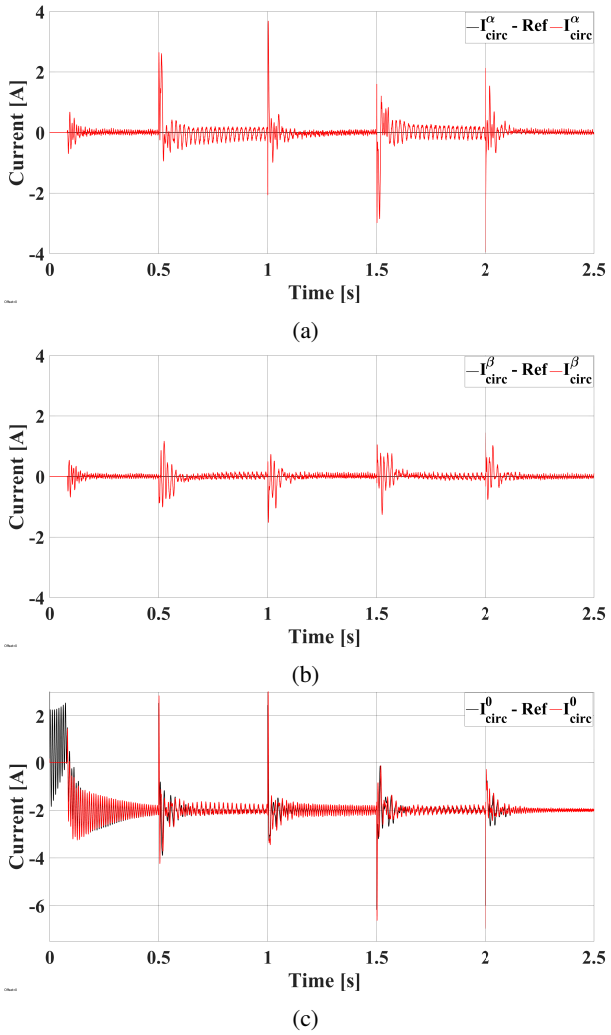

(a) (b) (c)

Fig. 7: (a) alpha, (b) beta, and (c) zero frame of circulating current using conventional method.

Then, at 1 second, SM-5 has another failure in the lower arm. When this fault occurs, it becomes symmetrical and lowers the voltage at phase-A by another level, from 8 to 7 level. The SMs are reinserted into the converter operation at 1.5 and 2 seconds, respectively, after the faults have been cleared. This outcome shows that the AC-PDPWM has undergone extensive testing in a three-phase system. However, as shown in Figure 5(b), the unbalanced SM voltages cause the AC-current component to circulate to the DC-side voltage.

The behavior of the SM voltage is shown in Figure 6. As seen in Figure 6(a), the healthy SM capacitor voltages at the leg of phase-A increase from 150 V to 200 V during the fault. The converter becomes an AF with unequal energy in the upper and lower at the leg of phase-A at 0.5 and 2

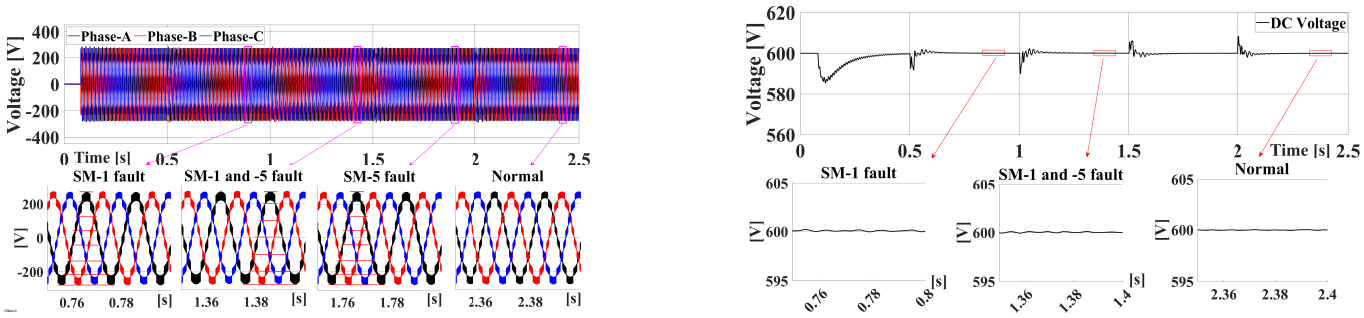

(a) (b)

Fig. 8: (a) The three-phase AC converter voltages and (b) the DC voltage using the proposed method.

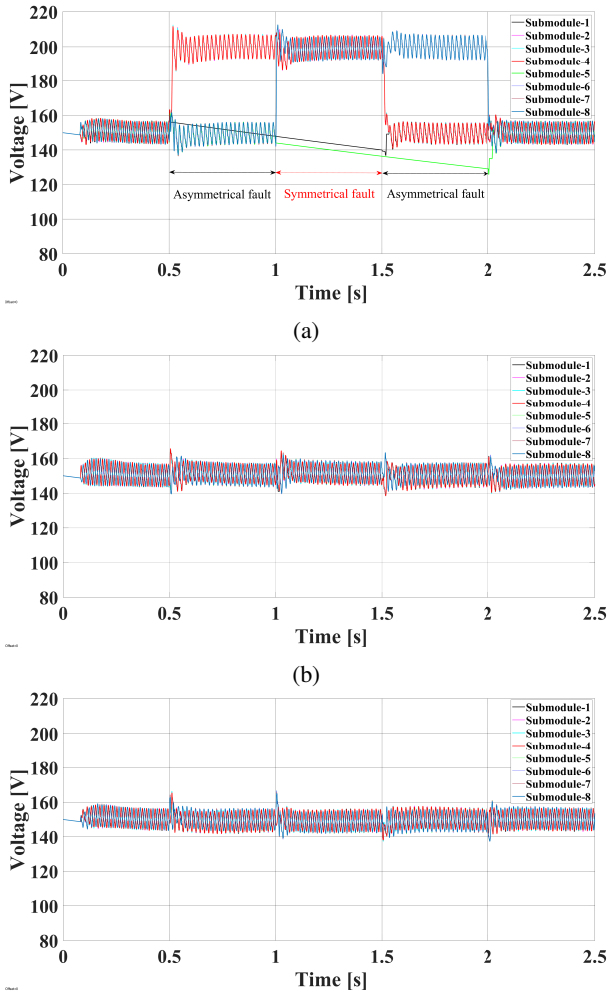

(a)

(b)

(c)

Fig. 9: SM capacitor voltages at (a) first leg, (b) second leg, and (c) third leg using the proposed method.

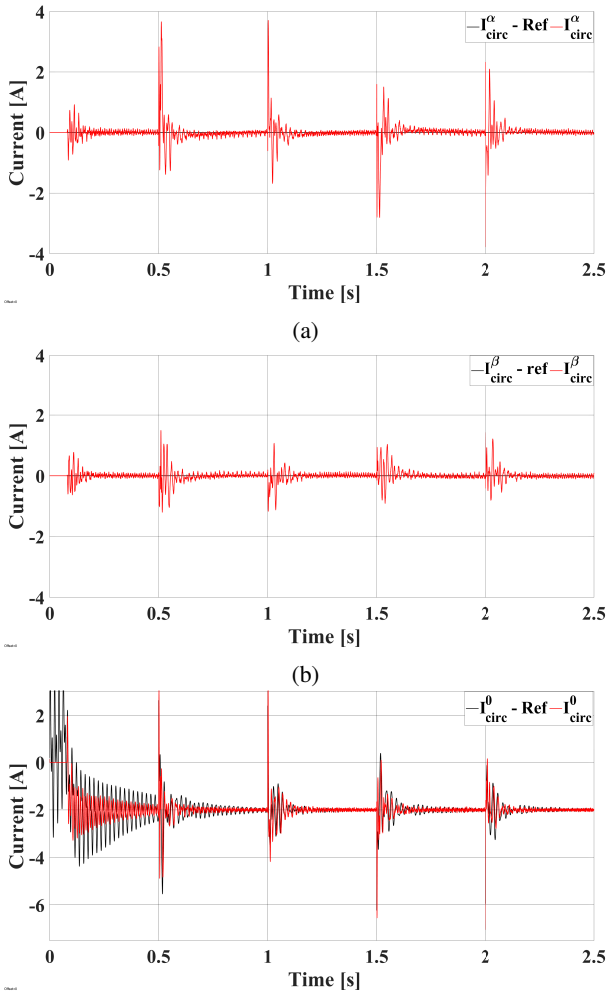

(a)

(b)

(c)

Fig. 10: (a) alpha, (b) beta, and (c) zero frame of circulating current using the proposed method.

seconds. The remaining SM voltages in the other arms and legs during the faults continued to behave normally, as seen in Figures 6(b) and 6(c). However, because of the imbalanced SM voltages, the conventional control is unable to remove the AC-current component that circulates within the leg. Figure 7 displays the analysis of the circulating current in each leg along the alpha-beta-zero frame axis. The fundamental AC-current component circulates throughout the arm when there is an energy difference between the upper and lower arms, as shown in Figure 7(b).

Figures 8-10 show the comparison results of the proposed method. The effectiveness of the proposed control in reducing the AC-current component of the circulating current during the

unbalanced or AF condition is also tested under the same fault conditions. The AC-current component in DC voltage can be well decreased, as seen in Figure 8(b).

The balance of aggregate and differential energy performance is better restored by the suggested control, as seen in Figures 9(a)-9(b). Figure 10 shows how, in contrast to conventional control, the fundamental AC-current component during the AF can be eliminated. The performance of DC voltage can be enhanced by lowering the flowing AC-current component in the alpha frame axis.

V. Conclusion

This work designed a control approach that would mitigate the issues arising from the internal SM failure in the three-phase MMC. The approach balances the internal power flow between the converter's arms during failure. To verify the design, MATLAB/Simulink was used to test symmetrical and asymmetrical faults for validation of the suggested internal voltage. The leg with the SM fault experiences the unbalanced voltage SM during the asymmetrical fault, but the AC-current component with fundamental frequency continues to circulate in the leg despite the application of fault tolerance, which preserves the stability of the converter. Even though the converter has an uneven voltage or energy SM, the suggested control approach can improve the converter's quality performance by removing the AC-current component during asymmetrical and symmetrical SM faults.

References

[1] M. A. Perez, S. Bernet, J. Rodriguez, S. Kouro, and R. Lizana, "Circuit topologies, modeling, control schemes, and applications of modular multilevel converters," *IEEE Transactions on Power Electronics*, vol. 30, no. 1, pp. 4–17, 2015.

[2] N. Ahmed, L. Ängquist, A. Antonopoulos, L. Harnefors, S. Norrga, and H.-P. Nee, "Performance of the modular multilevel converter with redundant submodules," in *IECON 2015 - 41st Annual Conference of the IEEE Industrial Electronics Society*, 2015, pp. 003 922–003 927.

[3] D.-H. Kim, J.-H. Kim, B.-M. Han, and Y.-D. Yoon, "Operational improvement of modular multilevel converter with redundancy submodules by new nlc scheme," in *2015 IEEE Power & Energy Society General Meeting*, 2015, pp. 1–5.

[4] G. Liu, Z. Xu, Y. Xue, and G. Tang, "Optimized control strategy based on dynamic redundancy for the modular multilevel converter," *IEEE Transactions on Power Electronics*, vol. 30, no. 1, pp. 339–348, 2015.

[5] J. Choi, B. Han, and H. Kim, "New scheme of phase-shifted carrier pwm for modular multilevel converter with redundancy submodules," *IEEE Transactions on Power Delivery*, vol. 31, no. 1, pp. 407–409, 2016.

[6] J. V. M. Farias, A. F. Cupertino, H. A. Pereira, S. I. S. Junior, and R. Teodorescu, "On the redundancy strategies of modular multilevel converters," *IEEE Transactions on Power Delivery*, vol. 33, no. 2, pp. 851–860, 2018.

[7] S.-M. Kim, K.-B. Lee, and J.-S. Lee, "Fault-tolerant control scheme for modular multilevel converter based on sorting algorithm without reserved submodules," in *2018 IEEE Applied Power Electronics Conference and Exposition (APEC)*, 2018, pp. 223–227.

[8] R. Darus, G. Konstantinou, J. Pou, S. Ceballos, and V. G. Agelidis, "Comparison of phase-shifted and level-shifted pwm in the modular multilevel converter," in *2014 International Power Electronics Conference (IPEC-Hiroshima 2014 - ECCE ASIA)*, 2014, pp. 3764–3770.

[9] H. Saad, X. Guillaud, J. Mahseredjian, S. Dennetière, and S. Nguefeu, "Mmc capacitor voltage decoupling and balancing controls," *IEEE Transactions on Power Delivery*, vol. 30, no. 2, pp. 704–712, 2015.

[10] T. B. Hashfi, S. Mekhilef, M. Mubin, M. Seyedmahmoudian, B. Horan, and A. Stojcevski, "Adaptive carrier-based pdpwm control for modular multilevel converter with fault-tolerant capability," *IEEE Access*, vol. 8, pp. 26 739–26 748, 2020.

[11] A. Elsanabary, T. B. Hashfi, S. Mekhilef, M. Seyedmahmoudian, and A. Stojcevski, "Submodule fault-tolerant control based adaptive carrier-pdpwm for modular multilevel converters," *Energy Reports*, vol. 7, pp. 7288–7296, 2021.

[12] P. Hu, D. Jiang, Y. Zhou, Y. Liang, J. Guo, and Z. Lin, "Energy-balancing control strategy for modular multilevel converters under submodule fault conditions," *IEEE Transactions on Power Electronics*, vol. 29, no. 9, pp. 5021–5030, 2014.

[13] H. Li, F. Deng, J. Zhao, J. Tian, Y. Lu, and G. Li, "Variable sampling frequency-based sm power loss balancing control for mmcs with bypassed faulty sms," *IEEE Transactions on Power Electronics*, vol. 38, no. 7, pp. 9006–9018, 2023.

[14] A. Elsanabary, S. Mekhilef, and N. Fadilah Ab Aziz, "Internal power balancing of an mmc-based large-scale pv system under unbalanced voltage sags," *IEEE Journal of Emerging and Selected Topics in Power Electronics*, vol. 12, no. 4, pp. 3729–3739, 2024.

[15] M. Parvez, M. F. M. Elias, N. A. Rahim, F. Blaabjerg, D. Abbott, and S. F. Al-Sarawi, "Comparative study of discrete pi and pr controls for single-phase ups inverter," *IEEE Access*, vol. 8, pp. 45 584–45 595, 2020.